Jurnal Media Mesin, Vol. 26 No. 1
Printed ISSN: 1411-4348
Online ISSN: 2541-4577

FRICTION PRESSURE PREDICTION OF SUPERCRITICAL CO_2 TURBULENT FLOW IN A CONCENTRIC ANNULUS

Md. Uddin
Department of Mechanical Engineering
Rajshahi University of Engineering & Technology, Rajshahi, Bangladesh
Email: msu@me.ruet.ac.bd

Md. Nahid Hossan
Department of Mechanical Engineering
Rajshahi University of Engineering & Technology, Rajshahi, Bangladesh
Email: nahid@me.ruet.ac.bd

Mim Mashrur Ahmed
Department of Mechanical Engineering
Rajshahi University of Engineering & Technology, Rajshahi, Bangladesh
Email: mashrur@me.ruet.ac.bd

Raihan Karal
Department of Mechanical Engineering
Rajshahi University of Engineering & Technology, Rajshahi, Bangladesh
Email: raihan.karal@me.ruet.ac.bd

ABSTRAK

Penelitian ini mengkaji lebih dalam visual gradien tekanan aksial dan karakteristik faktor gesekan dari aliran turbulen CO^2 superkritis dalam anulus konsentris dengan pendekatan numeris. Paket perangkat lunak dinamika fluida komputasi, CFD FLUENT digunakan untuk penyelidikan. Suhu saluran masuk bervariasi dari 31 hingga 110 $^{\circ}$C pada dua tekanan operasi 9 MPa dan 14 MPa. Pengaruh laju aliran massa, jarak anulus, dan kecepatan rotasi poros pada gradien tekanan dan faktor gesekan diselidiki. Hasil penelitian menunjukkan bahwa gradien tekanan bersifat non-linier dan faktor gesekan berubah secara tiba-tiba di dekat titik kritis. Pengaruh laju aliran massa dan kecepatan rotasi poros pada faktor gesekan ditemukan signifikan sedangkan efek jarak bebas tidak signifikan. Faktor gesekan untuk kondisi tertentu ditemukan dalam kisaran 0,042-0,029. Peningkatan satu setengah kali lipat dalam faktor gesekan ditemukan ketika ada peningkatan dua kali dalam kecepatan rotasi. Kesepakatan yang memuaskan diperoleh antara hasil yang diprediksi oleh CFD (fasih) jika dibandingkan dengan hasil yang diprediksi oleh persamaan Darcy Weisbach dan diagram Moody dan kemudian dengan eksperimental. Oleh karena itu, persamaan Darcy Weisbach dan diagram Moody dapat menjadi cara yang efektif untuk menentukan faktor tekanan dan gesekan masing-masing untuk aplikasi aliran turbulen CO_2 superkritis melalui anulus konsentris.

Kata kunci: CO_2 superkritis, aliran turbulen anulus, gradien tekanan, faktor gesekan, perbandingan.

ABSTRACT

This study uses a numerical approach to examine the visual axial pressure gradient and friction factor characteristics of supercritical CO_2 turbulent flow in a concentric annulus. The Computational Fluid Dynamics (CFD) software package (FLUENT) was applied for the investigation. The inlet temperature varied from 31 to 110 °C at two operating pressures 9 MPa and 14 MPa. The effect of mass flow rate, annulus clearance, and shaft rotational speed on the pressure gradient and friction factor are investigated. The results show that the pressure gradient is non-linear and the friction factor changes abruptly near the critical point. The effect of mass flow rate and shaft rotational speed on the friction factor is found significant whereas the effect of clearance is insignificant. The friction factor for a given condition is found in the range 0.042-0.029. A one-and-a-half times increase in the friction factor was found when there was a two-time increase in the rotational speed. A satisfactory agreement is obtained between the results predicted by CFD (fluent) when compared with the results predicted by the Darcy Weisbach equation and the Moody diagram and then with the experimental. Hence the Darcy Weisbach equation and Moody diagram can be an effective means of determining the pressure and friction factor respectively for the supercritical CO_2 turbulent flow application through the concentric annulus.

Keywords: *supercritical CO_2, annulus turbulent flow, pressure gradient, friction factor, comparison.*

1. INTRODUCTION

Supercritical CO_2 fluid has already been engaged in many applications such as the chemical industry, food industry, piping, heat exchange device, and turbo-machinery, and especially over the last decade, its application has been growing to develop power generation technologies [1]-[2]. The annulus flow is of great interest in those applications for component design and optimization [3].

The analysis of flow characteristics through the annulus has been conducted in earlier studies. A stationary cylinder's wall shear stress and annulus flow distribution at different Reynolds numbers for water have been studied. The wall shear stress and the gap flow velocity increased as the Reynolds number increased. There are differences in the axial and circumferential wall shear stress along the length [4]. The turbulent flow characteristics through the concentric annulus using direct numerical simulation have been studied. The results are compared for the different radius ratios at a fixed Reynolds number. The flow structures near the inner and outer walls have been investigated both physically and spectrally. The Reynolds shear stress has been conducted to understand the interaction among the boundary layer. The dynamics of Taylor vortices are also investigated [5].

The gas-liquid slug flow in a horizontal concentric annulus has been conducted and compared the simulation and experimental results. The pressure data has a strong dependence on mesh quality compared to slug frequency analysis [6]. The CFD study of the single-phase non-Newtonian power-law fluid flows through the horizontal rotating annulus has been conducted. The annulus radial clearance is 9.5 mm and the inner cylinder rotation is 400 rpm. The influence of the inner cylinder rotation on the pressure, flow behavior, and diameter ratio was investigated. The increasing inner cylinder rotation causes a negligible effect on the turbulent flow [7]. A CFD study of single-phase Newtonian fluid (water) flows through the horizontal rotating annulus has been conducted. The annulus radial clearance is 25 mm and the inner cylinder rotation is 150 rpm. The effect of pressure-velocity characteristics, the effect of the rotational speed, and the fluid concentration on the drilling application have been investigated [8].

The entrance region flow characteristics with Herschel-Bulkley fluids have been carried out for the rotating concentric annulus. The velocity distribution and pressure variation were obtained using finite difference analysis. The asymmetry characteristics found in the entrance region gradually reduced as the flow developed. The smaller the aspect ratio gives more stable flow characteristics [9]. The high Reynolds number turbulent velocity in a rotating Taylor Couette flow using image velocimetry has been measured. The effect of Reynolds number and viscosity on turbulent flow characteristics was investigated. The Reynolds stress components and dissipation rate were found to peak near the inner wall. At low viscosity, instantaneous vorticity fields were dominated, and at high viscosity, randomly distributed structures were generated [10]. The multi-phase (solid-liquid) non-Newtonian fluid flows through the vertical and inclined rotating annulus have been experimentally studied. The annulus radial clearance is 7 mm and the inner cylinder rotation is 600 rpm. The effect of inclination, rotation, flow velocity, and pressure was measured, and found that the increase in the particle feed concentration causes the increase in the pressure due to friction between the wall and the solids [11].

The radial distribution of the axial and tangential velocities together with friction factors as a function of the Reynolds number for two liquid fluids for the radius ratio of 0.50 has been presented. The friction factor increased by increasing inner body rotation. In turbulent flow, the axial velocity fluctuation decreases with increasing Reynolds number. At low Reynolds numbers and inner body rotation, the Taylor vortices produce complex flow patterns [12]. The Newtonian and non-Newtonian fluid flows through the concentric rotating annulus have been conducted. The annulus radial clearance is 10 mm and the inner cylinder rotation is 350 rpm. The effect of inner cylinder rotation on drag coefficient, axial velocity, and swirl profile has been investigated. The drag coefficient and axial velocity with and without rotation were found to be similar. The intensity of turbulent quantities is enhanced by the rotation particularly close to the inner wall. The effect of rotation with non-Newtonian fluid is similar to that of the Newtonian fluid but smaller in magnitude [13].

Most of the studies above investigated the pressure characteristics, velocity profile, wall shear, the effect of inner cylinder rotation, and the comparison of CFD results with the available literature. The studies were conducted for relatively greater clearance using single-phase and multiphase fluid flows. The fundamental study of supercritical CO_2 annulus flow has not been documented yet in the available literature. In this regard, the supercritical CO_2 turbulent flow analysis through the concentric annulus has been conducted in this study to fill up the knowledge gap on supercritical CO_2 fluid. The problem geometry and parameters have been adopted from the recent development of supercritical CO_2 power turbine configuration addressed in the literature [14]. The objective of this study is to investigate and document the turbulent flow behavior (pressure gradient and friction factor) of the supercritical CO_2 fluid for an annulus geometry. The effect of inlet temperature, operating pressure, clearance ratio, mass flow rate, and shaft rotational speed are investigated.

2. METHOD

The problem geometry, governing equation, boundary condition, and parameters are described in this section.

2.1 *Problem Geometry*

The horizontal annular geometry consisting of an inner shaft diameter of 76 mm, stationary outer wall thickness of 3 mm, and length of 152 mm (2D) formed a concentric layout [14]. The radial clearance is 1 mm.

The supercritical CO_2 enters the annulus at Z = 0 with axial uniform velocity (u = 0.15-1.0 m/s). The z-axis has been considered along the axial direction, and the x-axis along the radial direction is shown in Figure 1.

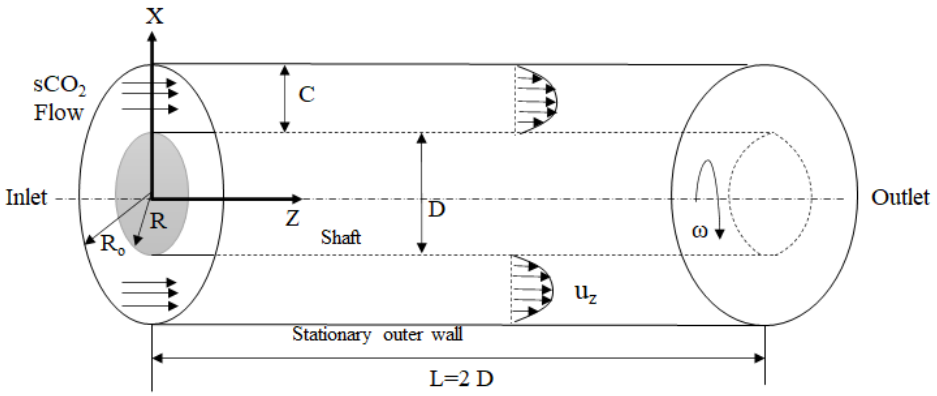

Figure 1. Schematic of The Problem Geometry

The National Institute of Standards and Technology (NIST) real gas properties for the supercritical CO_2 are used for the computation. The NIST real gas model has been activated by typing the text command at the Fluent console command prompt screen during the simulation and selecting the material. The NIST database employed the Helmholtz-energy equation of state for the computation.

2.2 *Governing Equation*

In this study, the Ansys fluent is employed for the simulation. The Ansys fluent solves the conservation equation of mass and momentum for the flow problems. The basic form of the mass conservation equation is as follows:

$$\frac{\partial \rho}{\partial t} + \nabla.(\rho \vec{u}) = 0 \tag{1}$$

The model considers fluid density, denoted as ρ, and fluid velocity vectors, represented as $\vec{u}$. These velocity vectors include components in the radial, axial, and tangential directions. Both parameters play a crucial role in defining the governing equations of fluid flow within the annular region, ensuring an accurate representation of momentum conservation and boundary conditions. The momentum conservation equation is as follows:

$$\frac{\partial}{\partial t}(\rho \vec{u}) + \nabla.(\rho \vec{u}\vec{u}) = -\nabla p + \nabla.(\bar{\bar{\tau}}) + \rho \vec{g} + \vec{F} \tag{2}$$

The model incorporates several key parameters: p represents the static pressure, τ denotes the stress tensor, ρg accounts for the gravitational body force, and F signifies the external body force. These factors collectively influence the fluid dynamics, governing the behavior of pressure distribution, stress interactions, and external influences within the system.

2.3 *Boundary Conditions and Parameters*

The boundary conditions for the model are defined as follows: At the annulus inlet (Z = 0), the velocity profile is uniform, expressed as $u(r) = u_{in}$ *for* $R < r < R_0$. At the annulus outlet (Z = L), the pressure is set to zero, denoted as $P = 0$ for $R < r < R_0$. The rotation boundary condition includes the absolute rotational velocity of the shaft, where the tangential velocity at the shaft surface is given by $\upsilon_\theta(R) = \omega R$, with ω representing the angular velocity of the shaft. A no-slip condition is applied at the shaft surface, ensuring $u(R) = 0$ and $\upsilon_\theta(R) = \omega R$. Additionally, system coupling is maintained at the interface between the shaft and the fluid, ensuring velocity and shear stress continuity. Gravity is neglected in this model, with $g = 0$. The conditions at the outer boundary $(r = R)$ may depend on whether the wall is stationary or allows slip, where R and R_0 are the shaft and outer wall radii, respectively.

The Reynolds number can be computed by the following expression [15]-[16].

$$\mathrm{Re}_a = \frac{\rho u D_H}{\mu}$$

$$\mathrm{Re}_{\omega} = \frac{\rho \omega R C}{\mu} \tag{3}$$

where Re_a and Re_ω are the axial and rotational Reynolds numbers respectively, ρ is the fluid density, u is the axial velocity, ω is the rotational velocity, D_H is the hydraulic diameter ($D_H = 2\ C$), μ is the dynamic viscosity of the fluid and C is the radial clearance. The friction factor in the stationary annulus ($\omega = 0$) can be computed by the following expression [15]:

$$f = \frac{4C}{\rho u^2} \times \left(\frac{dP}{L} \right) \tag{4}$$

where dP is the pressure drop in the annulus, L is the annulus length, and f is the friction factor in the annulus. The friction factor in the rotating annulus ($\omega \neq 0$) can be computed by the following expression [17]:

$$f = 0.26\left(\mathrm{Re}_a\right)^{-0.24} \times \left\{ 1 + \left(\frac{7}{8}\right)^2 \left(\frac{\mathrm{Re}_{\omega}}{2\mathrm{Re}_a} \right)^2 \right\}^{0.38} \quad (\mathrm{Re}_{\omega} > 10^4) \tag{5}$$

2.4 *Computational Mesh*

The Ansys workbench is employed to generate the computational mesh for the problem geometry shown in Figure 2. The hexahedral mesh element and the multi-zone mesh method are adopted to improve the mesh quality and better decomposition of the geometry. The inflation layer is added near the walls with a growth rate factor of 1.1 to ensure the accurate prediction of the near-wall parameters. The mesh-independent study is carried out to obtain the optimum number of mesh elements for the numerical solution.

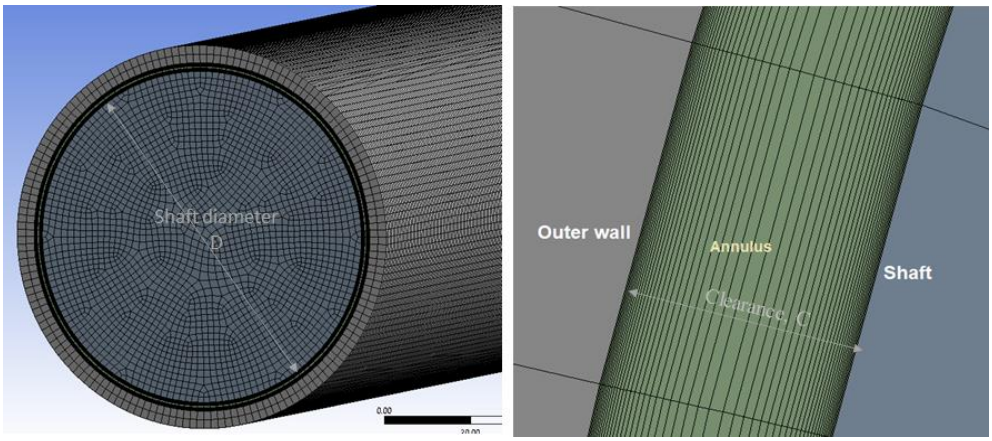

Figure 2. Computational Mesh Geometry

This study concerns the axial parameters and hence the variation of the axial pressure gradient for different axial divisions and mesh elements is shown in Table 1. It is seen that the axial pressure gradient remains unchanged as the number of axial divisions reaches 300. Hence, the number of axial divisions is 300 with a circumferential division is 160 and a radial division is 50, which satisfies the required mesh quality. The average orthogonality and skewness of the mesh are investigated and found to be 0.9951 and 0.0387 respectively which is in good agreement with the Ansys theory guide and the available literature [18]-[19].

Table 1. Mesh independent study (40°C and 9 MPa, $Re_a = 10^4$, $\omega = 0$, C = 1mm, k-ω model)

Number of axial division	Number of cells elements	Axial pressure gradient (Pa/m)
150	16,14,900	577.3
200	21,53,200	576.5
250	26,91,500	576.1
300	32,29,800	575.9
350	37,68,100	575.9

2.5 *Turbulent Model and Simulation Setup*

The pressure characteristics with different CFD turbulent models for the non-Newtonian fluid flow through the annulus geometry have been conducted in the literature [20]. They compared the CFD results with the experimental results shown in Figure 3 (a). The comparative analysis in Figure 3 (a) shows that the k-omega model provides accurate results for the flow through the concentric annulus.

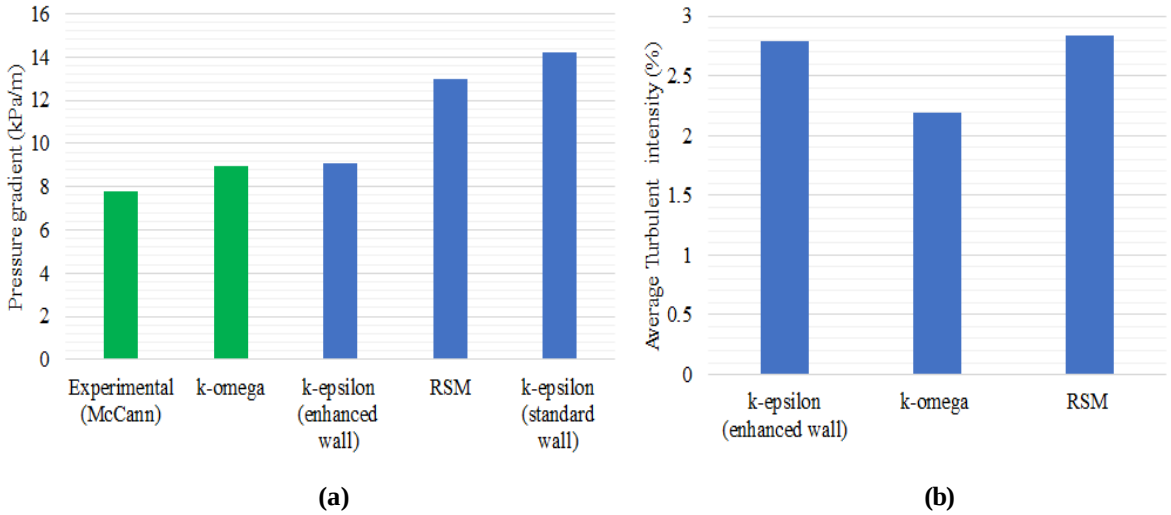

(a) **(b)**

Figure 3. Comparison of The Turbulent Model; Wall $y+ < 5$, $\Omega = 0$ (a) *Andrew And Salim, 2020* [20], C = 6.7 mm (b) Present Study, C = 1 mm

The present work investigated the turbulent intensity through the annulus shown in Figure 3 (b) to check the relative performance of the turbulent models for the supercritical CO_2 fluid. Figure 3 (b) shows the average turbulent intensity for different turbulent models. It is seen that the k-omega SST turbulence model gives lower intensity (2.19%) compared to the other turbulent models. It was reported that the model which gives higher turbulent intensity is called the worst-performing model while lower intensity corresponds to the most accurate model [20]. The difference in results among the models is due to the prediction of turbulent kinetic energy. The RSM model predicted the higher turbulent kinetic energy and thus higher turbulent velocity fluctuation gives higher turbulent intensity. Hence, the k-omega SST turbulence model can be considered the most accurate model for the supercritical CO_2 annulus flow and adopted in this study for further analysis.

The k-omega SST turbulent model and pressure-based steady-state solver have been employed to attain the numerical simulation. The simple procedure is introduced in the pressure-velocity coupling. The second-order upwind scheme is used to reduce the numerical error. The residual values of 10-4 are used as the convergence criteria during the simulation.

2.6 *Validation of the CFD Model*

The pressure gradient predicted by the CFD is compared with the pressure gradient obtained by the Darcy Weisbach equation [21] and the corresponding friction factor is compared with the friction factor read from the moody diagram to validate the CFD model. In addition, the CFD result is compared with the experimental results for a given condition. Figure 4 shows that the pressure predicted by CFD at different bulk temperatures and operating pressure are in very good agreement with the values calculated by the Darcy Weisbach equation at the same condition ($\omega = 0$, mass flow = 0.0253 kg/s, C = 1 mm). Moreover as shown in Figure 5, the Darcy Weisbach friction factor is in good agreement with the friction factor read from the Moody diagram. The CFD result is further compared with the experimental results [22] shown in Figure 6. In the experiment, the supercritical CO_2 fluid flows through the test section tube with pressure and flow rates were 8 MPa and 0.8 kg/min respectively. The temperature of CO_2 at the inlet and outlet of the test section is measured using the k-type thermocouple probe. The wall temperature is measured using a T-type thermocouple. The mass flow rate of the CO_2 is measured using a micro-motion mass flow meter. Assuming the annulus passage in this study is like a tube. The same condition is employed in the present geometry and the comparison of the predicted results shows that the CFD computed pressure drop has a good agreement with the experimental results.

Hence the Darcy Weisbach equation and Moody diagram can be employed to determine the pressure and friction parameters for the supercritical CO_2 annulus turbulent flow application. Also, the CFD simulation model can be considered reliable for further documentation. The sample velocity streamlines for the problem geometry are shown in Figure 7. It is seen that the streamline is straight with no rotation and the line becomes curved under rotation which is expected.

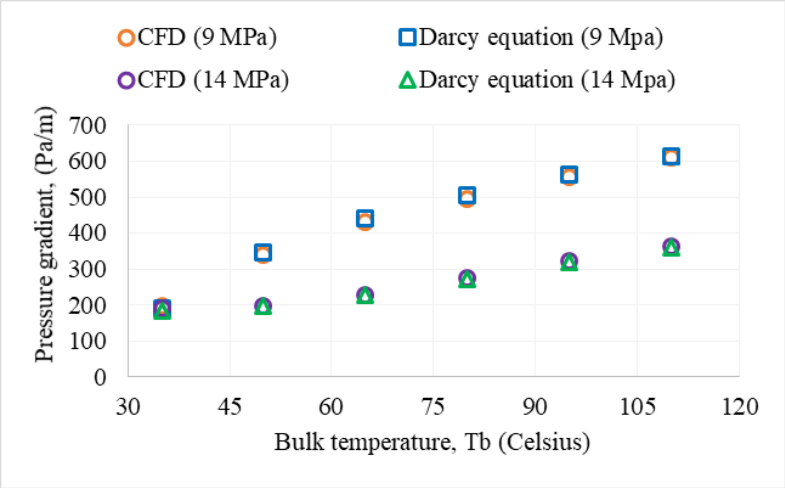

Figure 4. Comparison of the CFD Results with The Darcy Weisbach Equation (Ω = 0, Mass Flow rate m = 0.0253 kg/s, C = 1mm)

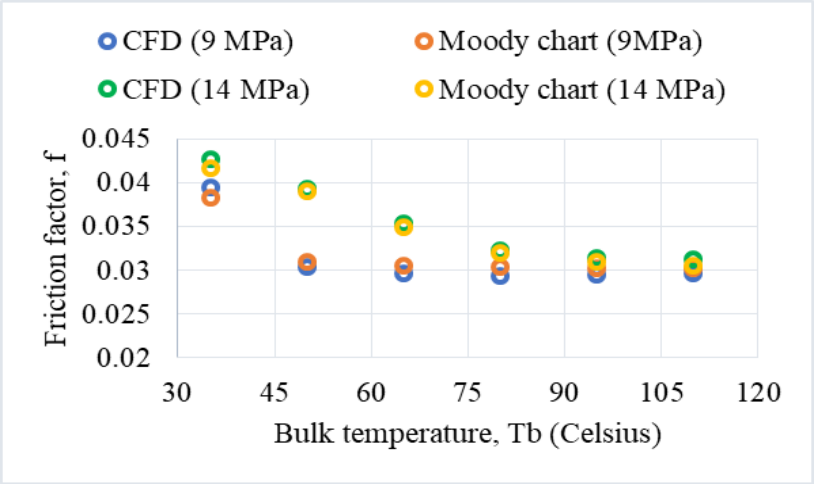

Figure 5. Comparison of The CFD Results with the Moody Diagram (Ω = 0, Mass Flow rate = 0.0253 kg/s, C = 1mm)

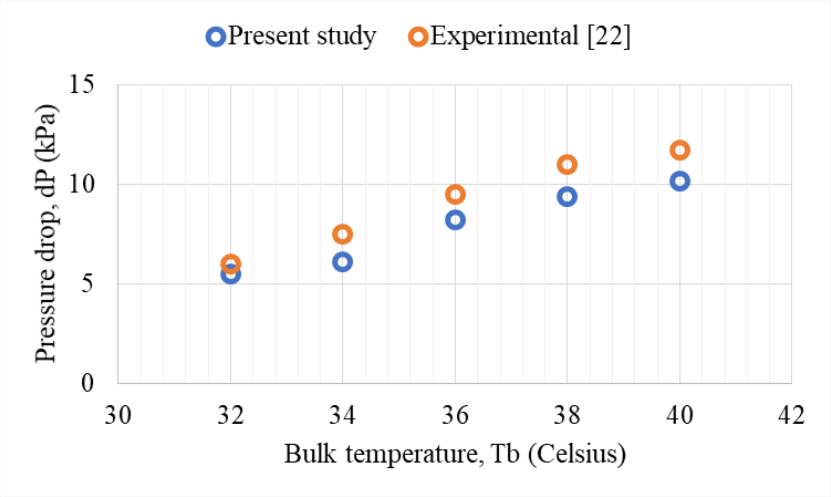

Figure 6. Pressure Drop Comparison between CFD and Experimental (Supercritical CO_2 Flow, 8 MPa, Mass Flow Rate m = 0.8 kg/min)

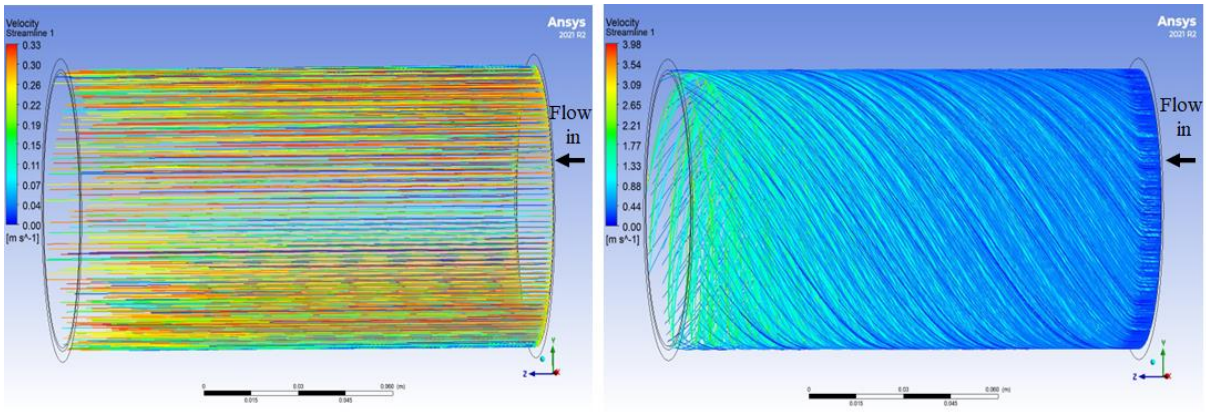

(a) **(b)**

Figure 7. Velocity Streamlines for The Problem Geometry, C = 1mm, m = 0.0253 kg/s (a) Ω = 0 (b) Ω = 1,000 RPM.

4. RESULTS AND DISCUSSION

The pressure gradient and friction factor predicted by CFD at different conditions are investigated and presented in this section.

4.1 *Pressure Gradient Characteristics*

Figure 8 shows the axial pressure gradient characteristics as a function of the temperature ratio (inlet temperature to critical temperature, Ti/Tc). It is seen that the pressure gradient increases non-linearly until the temperature ratio ≤ 1.10 and then increases almost linearly and more distinctly with the increasing temperature. The non-linear behavior of the pressure gradient near the critical condition is predicted and this is because the higher density of the fluid provides more resistance to change. The kinetic energy increases with increasing temperature for the same flow rate which causes more collisions of its molecules with the walls resulting in a greater force on the walls and a pressure gradient increase. In Figure. 8 (a), it is seen that the smaller the clearance ratio greater the pressure gradient. The effect of clearance is lower at a low temperature and becomes higher at a high temperature. The lower the operating pressure the higher the pressure gradient. The effect of operating pressure at near-critical conditions is found insignificant.

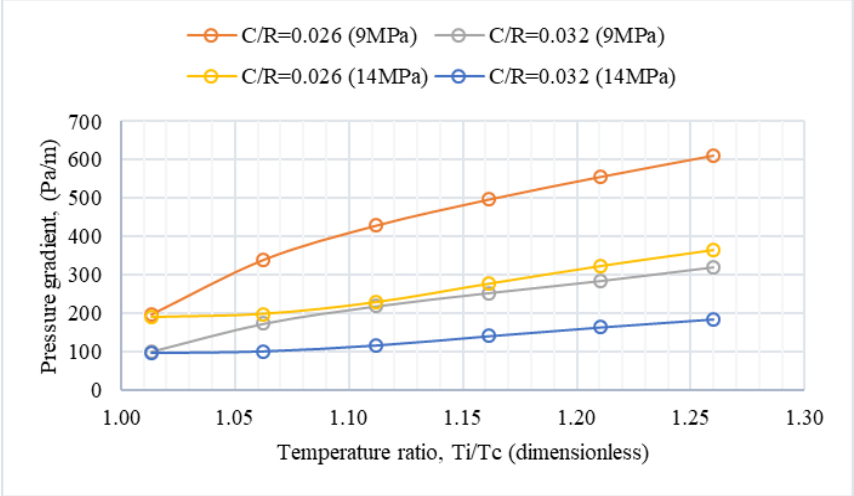

(a)

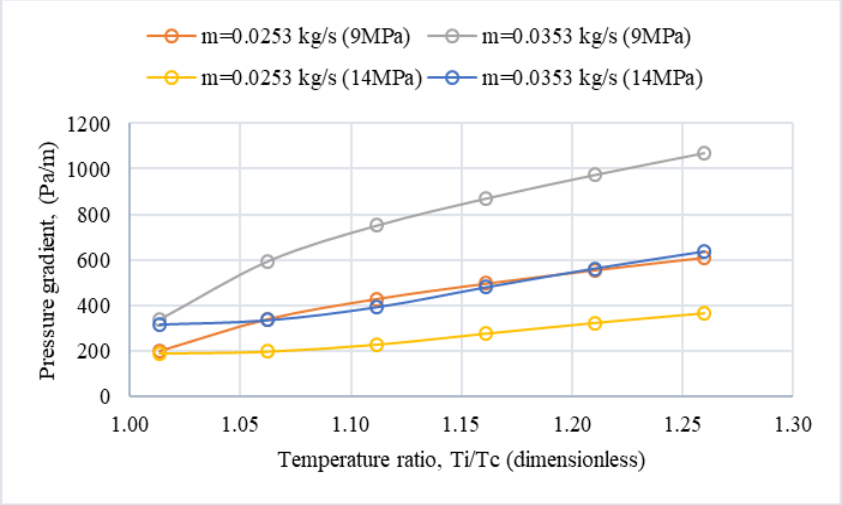

(b)

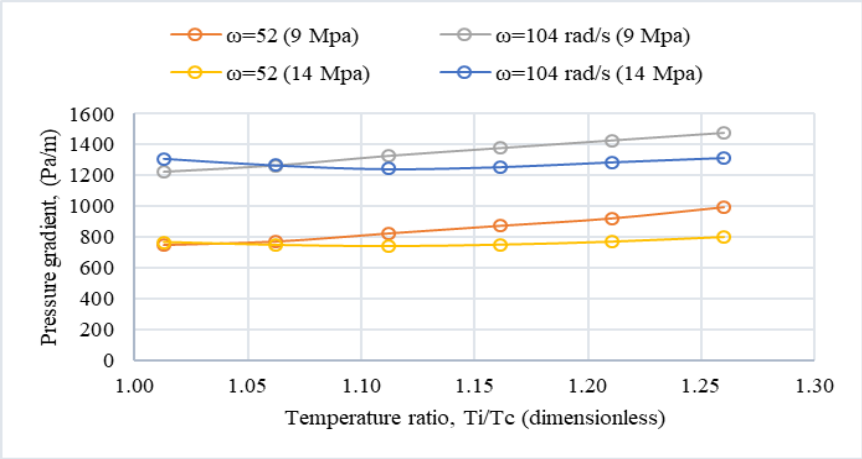

(c)

Figure 8. Pressure Gradient as a Function of The Temperature Ratio (a) Effect of Clearance Ratio; Ω = 0, m = 0.0253 kg/s (b) Effect of Mass Flow Rate; Ω = 0, C/R = 0.026 (c) Effect of Shaft Rotational Speed; m = 0.0253 kg/s, C/R = 0.026.

This is because the vapor condenses to liquid as the pressure increases in the sub-critical region and the changes in pressure have very little effect on the liquid. In Figure 8 (b), the pressure gradient increases with increasing mass flow rate. This is expected as the more mass flow rate means greater force exerted by the molecules and gives a greater pressure gradient. In Figure 8 (c), the pressure gradient increases with increasing shaft rotational speed. At low operating pressure, the pressure gradient is dominated by the rotating effect and changes are relatively steeper as the temperature ratio changes. At high operating pressure and low temperature, the pressure gradient is less dominated by the rotating effect due to the high density of the fluid. However, the rotating effect is observed at a higher temperature ratio ($T_i/T_c \geq 1.10$).

4.2 *Friction Factor Characteristics*

Figure 9 shows the Darcy friction factor characteristics as a function of the temperature ratio. It is seen that at a low temperature, the predicted friction factor is higher and decreases as the temperature increases. This is because the high-density fluid at a low temperature has a greater mass as well as greater force on the surface which results in higher friction. In Figure 9 (a), the effect of clearance is insignificant on the friction factor. The higher the operating pressure greater the friction factor. The higher and lower friction factors found are 0.042 and 0.031 respectively for the 14 MPa and 0.039 and 0.029 for the 9 MPa. In Figure 9 (b), the effect of mass flow rate on the friction factor is significant.

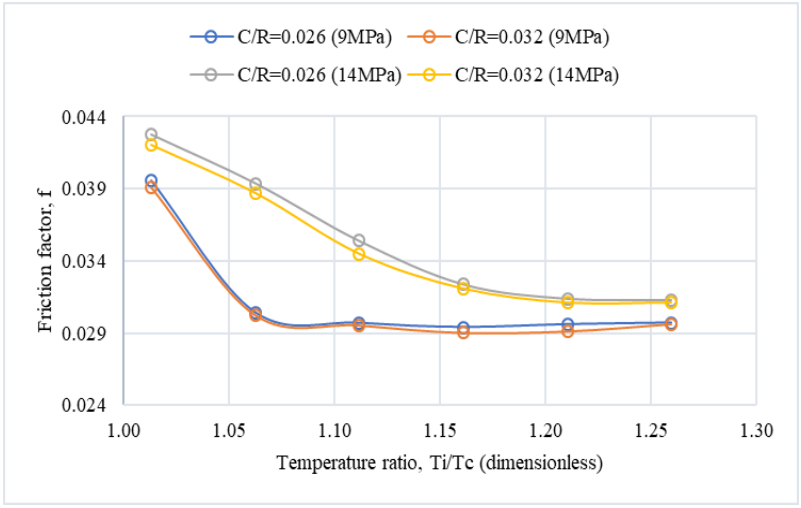

(a)

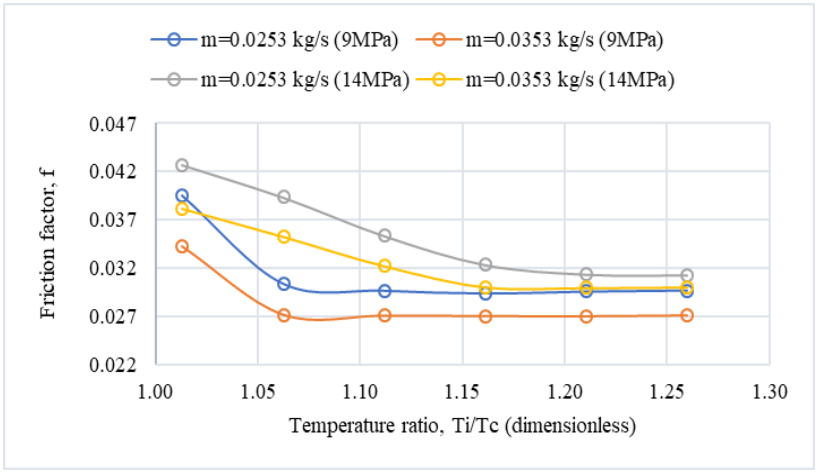

(b)

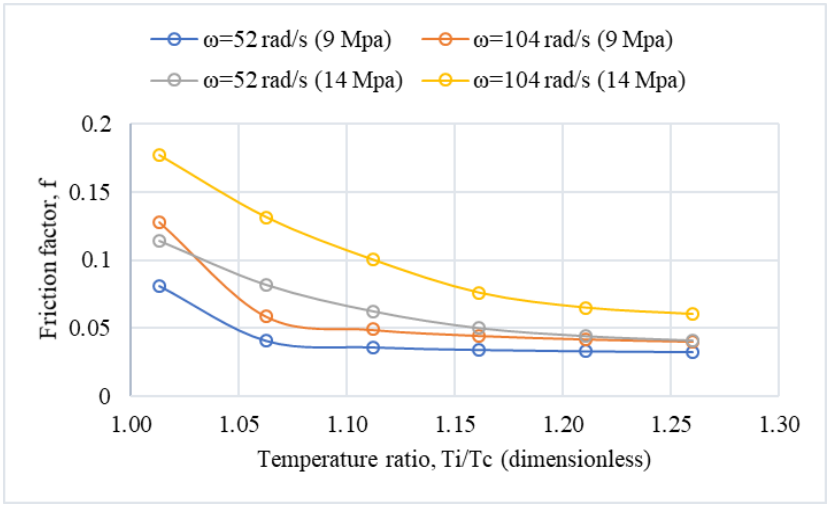

(c)

Figure 9. Darcy Friction Factor as a Function of The Temperature Ratio (a) Effect of Clearance Ratio; Ω = 0, m = 0.0253 kg/s (b) Effect of Mass Flow Rate; Ω = 0, C/R = 0.026 (c) Effect of Shaft Rotational Speed; m = 0.0253 kg/s, C/R = 0.026.

The higher the mass flow rate, lower the friction factor. This is because the higher the mass flow rate higher the fluid velocity which results in a lower friction factor. The higher friction factors found are 0.039 and 0.034 for the mass flow rate of 0.0253 kg/s and 0.0353 kg/s respectively at 9 MPa and 0.042 and 0.038 at 14 MPa. The lower friction factors found are similar. In Figure 9 (c), the effect of shaft rotational speed is also significant. The higher the rotational speed, the higher the friction factor. This is expected as the increase in the rotational speed leads to an increase in the radial effect on the flowing fluid and friction increase. It is seen that a 2 times increase in the rotational speed leads to a 1.5 times increase in the friction factor. At a low temperature, the distinction of the effect is significant whereas the effect is less significant at a high temperature.

5. CONCLUSIONS

The axial pressure gradient and friction factor characteristics of supercritical CO_2 turbulent flow through the concentric annulus have been investigated using the computational fluid dynamics (CFD) software package FLUENT. The effect of supercritical conditions (temperature and operating pressure) on the pressure gradient and friction factor has been studied. The effect of annulus clearance, mass flow rate, and shaft rotational speed has also been studied. The results obtained by CFD are compared with the results computed by the experiment. The following conclusion can be drawn:

1. The behavior of the pressure gradient near the critical condition is non-linear. The effect of operating pressure at near-critical conditions is found insignificant whereas a significant effect is predicted at a higher temperature.
2. The effect of the clearance ratio near the critical condition is insignificant. The pressure gradient is less dominated by the rotating effect at high operating pressure and low temperature.
3. The effect of operating pressure, mass flow rate, and shaft rotational speed on the friction factor are significant but the effect of clearance is insignificant.
4. The maximum and minimum pressure gradients found are 1,307 Pa/m and 100 Pa/m respectively for a given condition.
5. The maximum and minimum friction factors found are 0.042 and 0.029 respectively for a given condition. Two times increase in the rotational speed results in one and half times increase in the friction factor.
6. The friction factor predicted using the Darcy Weisbach equation agrees well with the friction factor read from the Moody diagram. So the Darcy Weisbach equation and Moody diagram can be used to predict the pressure and friction factor respectively for the supercritical CO_2 turbulent flow through the concentric annulus.

Currently, the fundamental analysis of supercritical CO_2 turbulent flow through the annulus geometry has not been studied. Hence, the study conducted in this paper will be very important for designing turbo-machinery components or another kind of high rotational speed apparatus with supercritical CO_2 fluid.

ACKNOWLEDGEMENT

The authors would like to thank the University of Queensland and the Australian Solar Thermal Research Institute (ASTRI) for funding and research facilities. Thanks are extended to Dr. Z. Guan and Dr. A. Klimenko for their technical help during the simulation. Thanks are also extended to Rajshahi University of Engineering & Technology (RUET), Bangladesh for providing sorts of facilities for manuscript preparation, review, editing, and submission.

REFERENCES

[1] G. Musgrove and S. Wright, "Fundamentals and Applications of Supercritical Carbon Dioxide (sCO_2) Based Power Cycles: Chapter 1: Introduction and Background," *Elsevier*, pp. 1–22, 2017, doi: 10.1016/B978-0-08-100804-1.00001-3.

[2] Q. Zhu, "Innovative power generation systems using supercritical CO_2 cycles," *Clean Energy*, vol. 1, no. 1, pp. 68–79, 2017, doi: 10.1093/ce/zkx003.

[3] A. Rahman, F. E. R. Corredor, M. Bizhani, and E. Kuru, "A CFD Simulation of Near Wall Turbulent Flow in Concentric Annulus," in *Proc. ASME 32nd Int. Conf. Ocean, Offshore and Arctic Eng*., Nantes, France, June 9–14, 2013.

[4] X. Jia, X. Sun, and J. Song, "Effect of Concentric Annular Gap Flow on Wall Shear Stress of Stationary Cylinder Pipe Vehicle under Different Reynolds Numbers," *Math. Probl. Eng*., Hindawi, 2020, pp. 1–19, doi: 10.1155/2020/1253652.

[5] E. Bagheri and B. C. Wang, "Effect of Transverse Curvature on Turbulent Concentric Annular Pipe Flow and Structures, "*11th International Symposium on Turbulence and Shear Flow Phenomena (TSFP11)* Southampton, UK, July 30 to August 2, 2019.

[6] C. Friedemann, M. Mortensena, and J. Nossen, "Gas-liquid slug flow in a horizontal concentric annulus, a comparison of numerical simulations and experimental data," *Int. J. Heat Fluid Flow*, vol. 78, no. 108437, pp. 1–14, 2019, doi: 10.1016/j.ijheatfluidflow.2019.108437.

[7] H. Ferroudji, A. Hadjadj, A. Haddad, and T. N. Ofei, "Numerical study of parameters affecting pressure drop of power-law fluid in horizontal annulus for laminar and turbulent flows," *J. Pet. Explor. Prod. Technol*., vol. 9, pp. 3091–3101, 2019.

[8] R. A. Sultan, M. A. Rahman, S. Rushd, S. Zendehboudi, and V. C. Kelessidis, "CFD Analysis of Pressure Losses and Deposition Velocities in Horizontal Annuli," *Int. J. Chem. Eng*., vol. 2019, Article ID 7068989, pp. 1–17, 2019.

[9] A. Kandasamy and S. R. Nadiminti, "Entrance Region Flow in Concentric Annuli with Rotating Inner Wall for Herschel–Bulkley Fluids," *Int. J. Appl. Comput. Math.*, vol. 1, pp. 235–249, 2015, doi: 10.1007/s40819-015-0029-7.

[10] R. V. Hout and J. Katz, "Measurements of mean flow and turbulence characteristics in high-Reynolds number counter-rotating Taylor-Couette flow," *Phys. Fluids*, vol. 23, no. 10, p. 105102, 2011, doi: 10.1063/1.3643738.

[11] S. M. Han, Y. K. Hwang, N. S. Woo, and Y. Kim, "Solid-liquid hydrodynamics in a slim hole drilling annulus," *J. Pet. Sci. Eng*., vol. 70, pp. 308–319, 2010.

[12] M. P. Escudier and I. W. Gouldson, "Concentric annular flow with center body rotation of a Newtonian and shear-thinning liquid," *Int. J. Heat Fluid Flow*, vol. 16, no. 3, pp. 156–162, 1995.

[13] J. M. Nouri and J. H. Whitelaw, "Flow of Newtonian and non-Newtonian fluids in a concentric annulus with the rotation of the inner cylinder," *ASME J. Fluids Eng.*, vol. 116, no. 4, pp. 821–827, 1994.

[14] S. Lee and H. Gurgenci, "A Comparison of Three Methodological Approaches for Meanline Design of Supercritical CO_2 Radial Inflow Turbines," *Energy Conv. Manag*., vol. 206, p. 112500, 2020, doi: 10.1016/j.enconman.2020.112500.

[15] R. C. McCann, M. S. Quigley, M. Zamara, and K. S. Slater, "Effects of high-speed pipe rotation on pressures in narrow annuli," *SPE Drill. Completion*, vol. 10, no. 2, pp. 96–103, 1995, doi: 10.2118/26343-PA.

[16] S. Grossmann, D. Lohse, and C. Sun, "High Reynolds number Taylor Couette Turbulence," *Annu. Rev. Fluid Mech.*, vol. 48, pp. 53–80, 2016.

[17] Y. Yamada, "Resistance of a flow through an annulus with an inner rotating cylinder," *Bull. JSME*, vol. 5, no. 18, pp. 302–310, 1962.

[18] I. E. Emmanuel and D. I. Gerogiorgis, "A multiparametric CFD analysis of multiphase annular flows for oil and gas drilling applications," *Comput. Chem. Eng*., vol. 106, pp. 645–661, 2017.

[19] Fluent Inc., Fluent 13 *User's Guide*, Canonsburg, PA, USA, 2010.

[20] A. A. Davidson and S. M. Salim, "CFD Modelling of Rotating Annular Flow using Wall y+," in *Trans. Eng. Technol*., Springer, pp. 318–330, 2020.

[21] F. M. White, *Fluid Mechanics*, 7th ed., eBook.

[22] Z. B. Liu, Y. L. He, Y. F. Yang, and J. Y. Fei, "Experimental study on heat transfer and pressure drop of supercritical CO_2 cooled in a large tube," *Appl. Therm. Eng*., vol. 70, pp. 307–315, 2014.